AFRL-RX-WP-TR-2014-0103

SILICA/ELECTRO-OPTIC POLYMER OPTICAL MODULATOR FOR MMW RECEIVING (PREPRINT)

Robert L. Nelson
AFRL/RXAS

MAY 2014
Interim Report

AIR FORCE RESEARCH LABORATORY
MATERIALS AND MANUFACTURING DIRECTORATE
WRIGHT-PATTERSON AIR FORCE BASE, OH 45433-7750
AIR FORCE MATERIEL COMMAND
UNITED STATES AIR FORCE

NOTICE AND SIGNATURE PAGE

Using Government drawings, specifications, or other data included in this document for any purpose other than Government procurement does not in any way obligate the U.S. Government. The fact that the Government formulated or supplied the drawings, specifications, or other data does not license the holder or any other person or corporation; or convey any rights or permission to manufacture, use, or sell any patented invention that may relate to them.

Qualified requestors may obtain copies of this report from the Defense Technical Information Center (DTIC) (http://www.dtic.mil)

AFRL-RX-WP-TR-2014-0103 HAS BEEN REVIEWED AND IS APPROVED FOR PUBLICATION IN ACCORDANCE WITH ASSIGNED DISTRIBUTION STATEMENT.

//SIGNED//
KATIE E. G. THORP, Program Mgr & Chief
Soft Matter Materials Branch
Functional Materials Division

//SIGNED//
KAREN R. OLSON, Deputy Chief
Functional Materials Division
Materials & Manufacturing Directorate

This report is published in the interest of scientific and technical information exchange and its publication does not constitute the Government's approval or disapproval of its ideas or findings.

REPORT DOCUMENTATION PAGE

Form Approved
OMB No. 0704-0188

1. REPORT DATE *(DD-MM-YY)*	2. REPORT TYPE	3. DATES COVERED *(From - To)*
May 2014	Interim	5 November 2009 – 27 December 2013

4. TITLE AND SUBTITLE
SILICA/ELECTRO-OPTIC POLYMER OPTICAL MODULATOR FOR MMW RECEIVING (PREPRINT)

5a. CONTRACT NUMBER
In-House

5b. GRANT NUMBER

5c. PROGRAM ELEMENT NUMBER
62102F

6. AUTHOR(S)
Oscar D. Herrera, Kyung-Jo Kim, Ram Voorakaranam, Roland Himmelhuber,
Robert A. Norwood, and Nasser Peyghambarian (University of Arizona)
Shiyi Wang and Qiwen Zhan (University of Dayton)
Li Li (TIPD LLC)
Jingdong Luo (Soluxra LLC)
Alex K.-Y. Jen (University of Washington)
Robert L. Nelson (AFRL/RXAP)

5d. PROJECT NUMBER
4347

5e. TASK NUMBER

5f. WORK UNIT NUMBER
X03Z (BN101100)

7. PERFORMING ORGANIZATION NAME(S) AND ADDRESS(ES)
AFRL/RXAS
3005 Hobson Way
Wright-Patterson AFB, OH 45433-7734

8. PERFORMING ORGANIZATION REPORT NUMBER

9. SPONSORING/MONITORING AGENCY NAME(S) AND ADDRESS(ES)
Air Force Research Laboratory
Materials and Manufacturing Directorate
Wright-Patterson Air Force Base, OH 45433-7750
Air Force Materiel Command
United States Air Force

10. SPONSORING/MONITORING AGENCY ACRONYM(S)
AFRL/RXAS

11. SPONSORING/MONITORING AGENCY REPORT NUMBER(S)
AFRL-RX-WP-TR-2014-0103

12. DISTRIBUTION/AVAILABILITY STATEMENT
Approved for public release; distribution is unlimited.

13. SUPPLEMENTARY NOTES
Approved by 88ABW Public Affairs Office: Case number 88ABW-2012-0846 on 17-February 2012. Report contains color.

14. ABSTRACT
A silica/electro-optic (EO) polymer phase modulator is proposed for millimeter-wave (MMW) radiation receiver with the use of a bowtie antenna. Waveguide design optimization is presented for a waveguide with an EO polymer core and silica/solgel cladding. Electrode effects on the insertion loss and poling efficiency are also analyzed and conditions for low-loss and high poling efficiency established. The bowtie antenna is simulated and shows a broadband response with a maximum at 5GHz and a 3dB-bandwidth of approximately 12GHz. A fiber splicing technique is presented that reduces coupling loss between SMF-28 and the waveguide. Experimental results for a fabricated device with MMW-response between 10-14GHz are shown with carrier to first sideband intensity difference of up to -36dB.

15. SUBJECT TERMS
electro-optic modulators, optical waveguides, optical polymers, millimeter wave detection

16. SECURITY CLASSIFICATION OF:			17. LIMITATION OF ABSTRACT:	18. NUMBER OF PAGES	19a. NAME OF RESPONSIBLE PERSON (Monitor)
a. REPORT	b. ABSTRACT	c. THIS PAGE			Katie E. G. Thorp
Unclassified	Unclassified	Unclassified	SAR	11	19b. TELEPHONE NUMBER *(Include Area Code)* (937) 255-9159

REPORT DOCUMENTATION PAGE (Cont'd)

7. PERFORMING ORGANIZATION NAME(S) AND ADDRESS(ES)

University of Arizona
Tucson, AZ 85721

University of Dayton
Dayton, OH 45469

TIPD LLC
Tucson, AZ 85705

Soluxra LLC
Seattle WA 98195

University of Washington
Seattle, WA 98195

AFRL/RXAS
3005 Hobson Way
Wright-Patterson AFB, OH 45433

Silica/Electro-optic Polymer Optical Modulator for MMW Receiving

Oscar D. Herrera, Kyung-Jo Kim, Ram Voorakaranam, *Member, IEEE,* Roland Himmelhuber, Shiyi Wang, Qiwen Zhan, Li Li, Robert A. Norwood, *Member, IEEE,* Robert L. Nelson, Jingdong Luo, Alex K.-Y. Jen, and Nasser Peyghambarian

***Abstract*—A silica/electro-optic (EO) polymer phase modulator is proposed for millimeter-wave (MMW) radiation receiver with the use of a bowtie antenna. Waveguide design optimization is presented for a waveguide with an EO polymer core and silica/sol-gel cladding. Electrode effects on the insertion loss and poling efficiency are also analyzed and conditions for low-loss and high poling efficiency established. The bowtie antenna is simulated and shows a broadband response with a maximum at 5GHz and a 3dB-bandwidth of approximately 12GHz. A fiber splicing technique is presented that reduces coupling loss between SMF-28 and the waveguide. Experimental results for a fabricated device with MMW-response between 10-14GHz are shown with carrier to first sideband intensity difference of up to -36dB.**

***Index Terms*—electrooptic modulators, optical waveguides, optical polymers, millimeter wave detection**

I. Introduction

THE detection of high frequency electromagnetic fields, in particular millimeter-wave (MMW), has been heavily studied for wireless data transfer. Currently, various horn antennas for the detection of near-field signals are used as probes [1]. These are purely electronic techniques, that are limited by their large metallic structure and the coaxial cables used to connect them which can introduce noise. Furthermore, their large size is a limiting factor for their incorporation into small equipment and large arrays with sufficient sensitivity for passive imaging.

O.D. Herrera is with the University of Arizona, Tucson, AZ, 85721 USA (e-mail: oherrera@optics.arizona.edu)

K. Kim is with the University of Arizona, Tucson, AZ, 85721 USA (e-mail: kkim@optics.arizona.edu).

R. Voorakaranam is with the University of Arizona, Tucson, AZ, 85721 USA (e-mail: ram@optics.arizona.edu).

R. Himmelhuber is with the University of Arizona, Tucson, AZ, 85721 USA (e-mail: rolandh@optics.arizona.edu).

S. Wang is with the University of Dayton, Dayton, OH, 45469 (e-mail: wangs6@udayton.edu).

Q. Zhan is with the University of Dayton, Dayton, OH, 45469 (e-mail: qzhan1@udayton.edu).

L. Li was with TIPD LLC, Tucson, AZ, 85705, USA. He is now with Nanjing University of Science and Technology, Nanjing, 210094, P.R. China (e-mail: lili@njust.edu.cn).

R.A. Norwood is with the University of Arizona, Tucson, AZ, 85721 USA (e-mail: rnorwood@optics.arizona.edu).

R.L. Nelson is with the Air Force Research Laboratory at Wright Patterson, Dayton, Ohio 45433, USA (email: robert.nelson.21@us.af.mil).

J. Luo is with Soluxra LLC, Seattle, WA 98195 USA (email: jingdong.luo@soluxra.com).

A. K.-J. Jen is with the University of Washington, Seattle, WA 98195 USA (email: ajen@u.washington.edu).

N. Peyghambarian is with the University of Arizona, Tucson, AZ, 85721 USA (e-mail: Nasser@optics.arizona.edu).

To circumvent these issues, photonic techniques for detection of MMW signals have been proposed. In many cases they incorporate the use of $LiNbO_3$-based optical waveguide modulators as probes. The measurement techniques include direct intensity modulation by the incorporation of a Mach-Zender modulator design [2] or measurement of the optical power of the sidebands on the optical input which correlate with the power of the MMW radiation driving the phase modulator [3]. The detection and driving mechanism can be a horn-antenna [4], [5] or embedded antenna with coplanar waveguide electrodes fabricated on the EO crystal substrate [6], [7], [8], [9].

Polymer-based EO modulators are capable of ultrafast modulation with bandwidth up to 1.6THz [10] because of their intrinsically fast electronic response. In the hybrid polymer/sol-gel device approach, an in-device EO coefficient (r_{33}) as large as 170 pm/V has been achieved [11], as well as highly efficient, sub-volt drive voltage [12], [13]. Furthermore, thin film EO polymers can be spun onto any desired substrate which is advantageous in cases such as ion-exchange glass waveguides for low insertion loss [14] or silicon for silicon photonics integration [15]. For the case of RF detection, a low-k dielectric substrate is desired to provide low MMW signal distortion. Also, the size of the antenna is $\propto 1/\sqrt{\varepsilon_{\text{eff}}}$; therefore, a low-$k$ substrate would allow for a larger antenna and higher received power.

In this paper we present a MMW receiver that uses a silica/EO polymer phase modulator with pigtailed optical fibers. We propose waveguide and electrode designs for enhancing the electro-optic effect and achieving low metal absorption of the optical carrier. Bowtie antenna simulations are shown to demonstrate the expected field enhancement of the device. A novel fiber splicing technique is presented to reduce coupling loss between SMF-28 fiber and the waveguide. A pigtailed device is fabricated and tested with MMW-response between 10-14GHz. This device requires no complex fabrication techniques, it is compact and is the first EO polymer-based MMW receiver to our knowledge.

II. Signal Conversion

Most electro-optic modulators rely on the change of the refractive index produced from the application of an electric field[16]. The change in index is proportional to the applied electric field (Pockels effect). The applied field on an EO polymer thereby modifies the incident polarized light passing

through it by inducing a phase change. The induced index change, $\Delta n(t)$, by an applied voltage, $V(t)$, in an EO polymer waveguide is defined as,

$$\Delta n(t) = \frac{1}{2} r_{33} n_{\text{eff}}^3 \Gamma \frac{V(t)}{d}, \quad (1)$$

where r_{33} is the electro-optic coefficient, n_{eff} is the effective refractive index of the propagating mode, Γ is the overlap integral factor defined as the convolution of the guided mode with the applied electric field in the EO material, and d is the electrode separation. The net phase change, $\Delta\phi$, for a modulator of length L is

$$\Delta\phi(t) = 2\pi \Delta n(t) \frac{L}{\lambda}, \quad (2)$$

where λ is the wavelength of the optical signal in the EO polymer waveguide. Assuming that the output optical field, E_0, undergoes a sinusoidal modulation voltage at a frequency ω_m then the output optical field can be expressed as [17],

$$\begin{aligned} E_0 &= E_i \exp[i(\omega_0 t + \Delta\phi)] \\ &= E_i \exp[i(\omega_0 t + m\cos(\omega_m t))], \end{aligned} \quad (3)$$

where E_i is the input optical field and m is the modulation index defined as,

$$m = \pi \frac{V_m}{V_\pi}, \quad (4)$$

where V_m is the peak modulation voltage and V_π is the voltage necessary to induce a full π phase shift and is defined by the properties of the modulator as,

$$V_\pi = \frac{\lambda d}{r_{33} n_{\text{eff}}^3 L \Gamma}. \quad (5)$$

In the frequency domain, the drive voltage perturbs the optical spectrum characteristics of the output signal. Through Fourier analysis [17] one can derive the output intensity in the frequency domain. The resulting spectrum consists of a carrier component and an infinite number of sidebands all related to different order Bessel functions. The first sidebands are located to the red and blue of the optical carrier frequency with the shift being given by the driving frequency of the modulator ω_m. Because we are interested in the detection of small modulation signals ($m \ll 1$), a small signal approximation and Taylor expansion to the first order may be used and the intensity of the first order sidebands (I_{FSB}) can be approximated as,

$$I_{FSB} = I_i \left(\frac{m}{2}\right)^2. \quad (6)$$

From (4) and (6), it can be inferred that the intensities of the first order sidebands are directly proportional to V_m. In the case of an EO modulator used as a MMW receiver, V_m is related to the intensity of the MMW signal detected by the antenna. Therefore, one could define a conversion efficiency of a MMW phase modulator receiver as the difference between the intensities from the carrier component and the first sidebands.

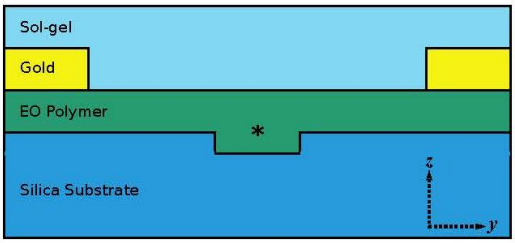

Fig. 1. Silica/EO polymer waveguide design. Waveguide width and EO polymer thickness of the core are 3.5μm. The center of the waveguide is defined by the black asterisk ($z = 0$).

III. Modulator Design

A. Waveguide

Our waveguide design for 1550nm light comprises an EO polymer as the core ($n \approx 1.7$) and silica as the bottom and side cladding ($n = 1.44$). Silica was chosen over silicon as a substrate because of its dielectric constant is much lower than silicon's. Even though silicon is the most common substrate for integrated optics, its high dielectric constant ($\epsilon_{\text{Si}} \approx 12$ at microwave frequencies) can result in large reflections of the MMW signal of interest, while silica's lower dielectric constant ($\epsilon_{\text{SiO}_2} \approx 3.9$ at microwave frequencies) results in much lower reflections.

The design is shown in Fig. 1. The waveguide is composed of a 1μm deep trench in the silica substrate with 3.5μm thick EO polymer as the core (2.5μm away from the trench). The top cladding is composed of 10μm of in-house sol-gel ($n = 1.486$). Waveguide simulations were performed using commercial software Fimmwave 5.1. The waveguide maintains single mode propagation for waveguide widths $\leq 4.5\mu$m. For a waveguide width between $2.5 - 4.5\mu$m the mode field diameter was within $4.8 - 4.5\mu$m, the TE confinement was ~ 0.99 and n_{eff} was between 1.683 and 1.685. The electric field of the TE mode for the proposed design is shown in Fig. 2. The mode field diameter is 4.55μm.

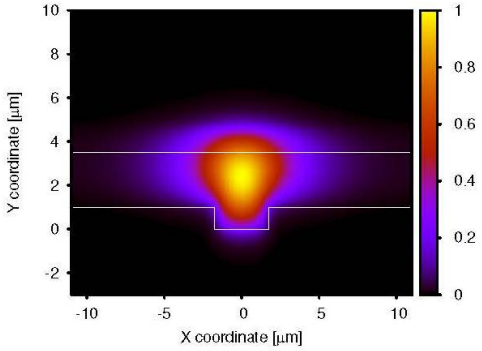

Fig. 2. Electric field of a TE mode in the silica/EO polymer waveguide. The waveguide width is 3.5μm and trench depth is 1μm.

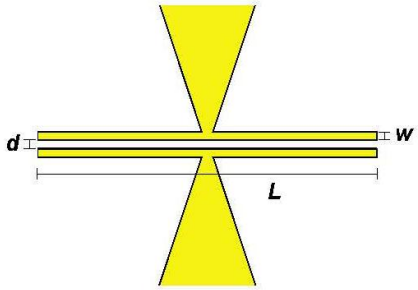

Fig. 3. Electrode design for MMW antenna with electrode length $L = 1.2$mm, width $w = 10\mu$m, and separation $d = 10\mu$m.

B. Electrode Design

The MMW to light wave conversion is attained through an optical phase modulating process. To efficiently convert MMW signals, the EO polymer must be properly poled such that the largest electro-optic effect is achieved. This design requires a coplanar-strip electrode geometry for both poling the polymer and the MMW-optic field conversion. The electrodes are symmetrically connected to the tip of the bow-tie antenna as shown in Fig. 3. The electrode length is 1.2mm, width is 10μm and separation is 10μm. Optical loss due to the metal (gold) absorption was simulated with respect to electrode separations for different waveguide widths. The electrode thickness was 2μm and length $L = 1.2$mm. Losses due to electrode absorption improved as the waveguide width was increased and also as the electrode separation increased. For electrode separation $d > 7\mu$m the electrode loss was < 0.1dB for waveguide widths ranging from 2.5-4.5μm.

Simulations of the DC electric field between the electrodes were conducted using COMSOL 4.3a. Fig. 4 displays the DC field between two electrodes separated by 10μm with the waveguide in the center. The scale of the field is normalized to the effective field expected from a microstrip geometry for electrodes with equivalent electrode separation. In a microstrip geometry, the expected field between the electrodes is the applied voltage divided by the separation (i.e. as in a simple capacitor). One can see that the field within the EO polymer region is relatively uniform to $\sim$70% of an equivalent microstrip in this electrode configuration. This field uniformity is beneficial to both the effective index change and the poling of the polymer. Table. I reviews all the thickness and refractive index parameters for the waveguide design as well as some material properties.

TABLE I
MATERIAL PROPERTIES FOR DEVICE

Material	Values
SEO100 EO polymer	
- Refractive index (TE poled)	1.7
- Dielectric constant, ϵ_{EO}	3.2
- Thickness(in waveguide region)	$\sim 3.5\mu$m
95/5 Sol-gel	
- Refractive index	1.486
- Dielectric constant, ϵ_{SG} (at 10GHz)	~ 4
- Thickness	10μm
Fused Silica	
- Refractive index	1.44
- Dielectric constant, ϵ_{SiO_2}	4
- Etch depth	1μm

IV. ANTENNA DESIGN AND MODELING

A bowtie antenna design was used to receive the MMW radiation with the dimensions shown in Fig. 5. A three-dimensional finite-element-method (COMSOL Multiphysics) model is built to study the RF response of the bowtie antenna integrated with the EO polymer/silica waveguide. An RF plane wave polarized in the y-direction (see Fig. 1) illuminates the structure at normal incidence from the sol-gel side. The field enhancement (FE) factor is defined as the resonant electric field inside the gap region divided by the incident field. Fig. 6

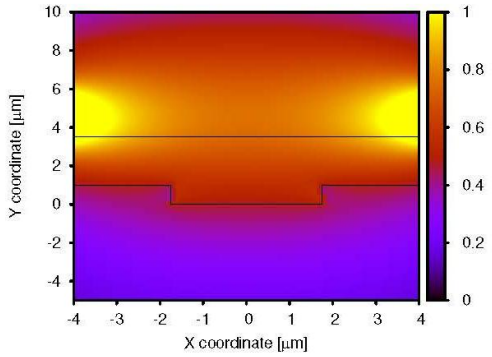

Fig. 4. Simulated DC field between 10μm separated electrodes. Electrode thickness is 2μm.

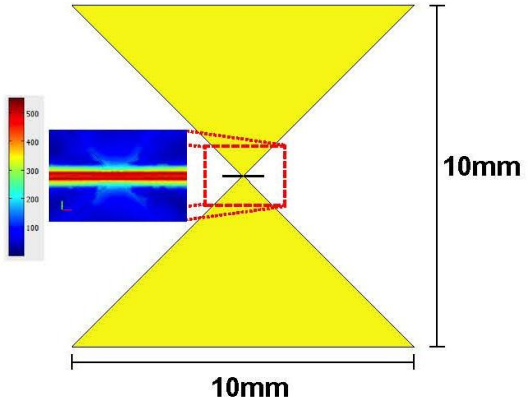

Fig. 5. Bowtie antenna design with dimensions. A top view of the field enhancement distribution near the gap region at the EO polymer/silica substrate interface ($z = 0$) is shown in the inset.

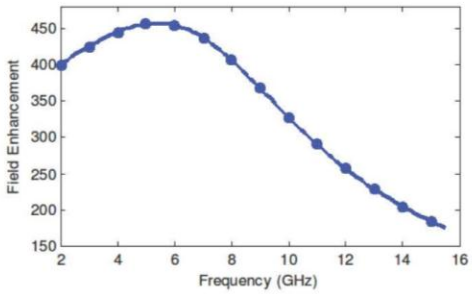

Fig. 6. Field enhancement factor monitored at the center of the EO polymer waveguide versus the input RF frequency showing an extremely broadband response with peak at 5 GHz.

shows the FE factor measured at the center of the waveguide (black asterisk in Fig. 1) versus the RF frequency. These simulation results show that the compressed RF radiation is enhanced by a factor of 450 at 5 GHz and by a factor of 300 at 10 GHz inside the EO polymer waveguide. An RF 3dB-bandwidth of approximately 12 GHz is also observed. It should be noted that the FE factor would be much higher (>1000) at regions close to the corners of electrodes. However, the overlap between the enhanced RF field and the optical mode will mainly occur in the center region of the gap. Consequently, we choose the FE factor in the center of the EO polymer waveguide to characterize the device performance.

The electric field pattern at 5 GHz across the entire bowtie antenna was also simulated and a dipolar type resonance was clearly identified. The FE distribution within the antenna gap region at the $z = 0$ plane is shown in Fig. 5[inset], and demonstrates a fairly uniform FE distribution for the area where most of the overlap with the optical mode will occur. Fig. 7 shows the FE factor profiles for both 5 GHz and 10 GHz across the device in the vertical direction (along the z-axis through the black asterisk of Fig. 1). It can be seen that the FE factor is the highest in the plane of the bowtie antenna electrodes and decreases away from it. Thus it would be beneficial if the optical mode profile is designed to be closer

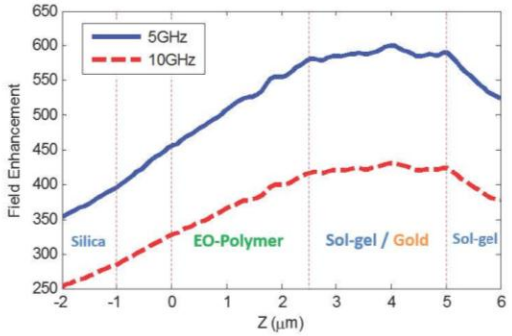

Fig. 7. Field enhancement profiles at 5 GHz and 10 GHz across different layers at the center of the device.

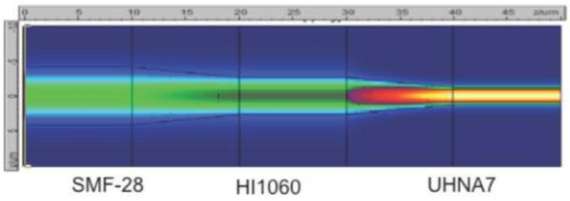

Fig. 8. Modeled light propagation from SMF-28 to UHNA7 fiber

to the EO polymer/sol-gel interface.

V. Fiber Coupling

Fiber coupling simulations using Fimmwave were conducted for the waveguide using SMF-28 (mode field diameter of ~10.5μm). The use of SMF-28 would result in a coupling loss of ~3dB per interface (total of ~6dB) due to the mode diameter differences between the waveguide and fiber. High numerical aperture fibers, such as UHNA7 (mode field diameter ~3.2μm), give lower coupling losses per interface to resulting in total coupling loss of 1.6dB. A robust fiber splicing approach to transition from SMF-28 to UHNA7 using HI-1060 fiber was developed with a total transition loss of about 0.4dB. This approach is modeled in Fig. 8. By adopting this transition method the total coupling loss is reduced to ~2.4dB.

The fiber transitions were fabricated and tested using UHNA1 high NA fiber [Thorlabs] with a mode field diameter of 4.8 at 1550nm. This high NA fiber was used in order to overlap better with the waveguide mode size. A loss of ~0.5dB was measured for a transition from SMF-28 to UHNA1. The packaging approach assumes that the antenna device will be diced using a special glass foot for support. Optimized UV epoxies are used to attach the glass ferrule to the chip. These UV epoxies have been shown to withstand high optical power (> 100mW) in previous measurements.

VI. Experiment

A. Fabrication

A fused silica wafer with a thickness of 500μm was used as the waveguide substrate. A 2.5μm wide waveguide trench was exposed on the wafer through UV-lithography using a Karl Suss MA6 mask aligner and S1813 photoresist. The exposed areas were etched by reactive ion (RIE) etching using an Oxford Plasma 100 RIE and CF_4 gas. The photoresist was later removed with acetone and cleaned with isopropyl alcohol. Before spinning the EO polymer, an adhesion promoter is needed to improve adhesion between the EO polymer and the silica substrate. The adhesion promoter is 3-aminopropyltrimethoxysilane and had a thickness no greater than 10nm. This made a significant improvement in the handling of the samples during later fabrication processes. The samples were spun with EO polymer SEO100 (from Soluxra) for a thickness of 2.5μm. These samples were then dried at 80°C under vacuum for 16 hours.

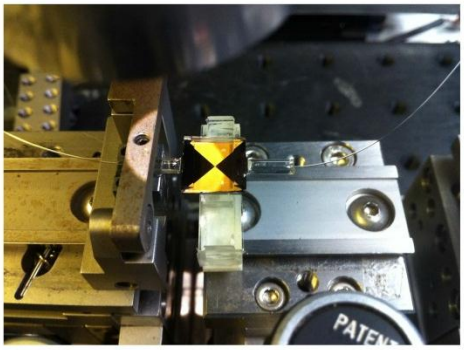

Fig. 9. Pigtailed antenna with UHNA1-SM28 transition fiber.

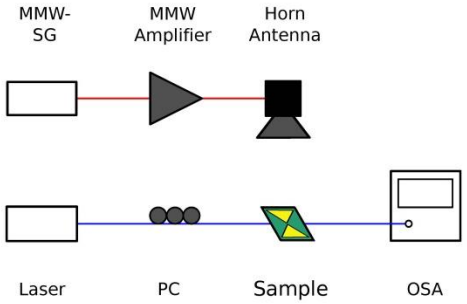

Fig. 10. Experimental setup for measuring SiO_2/EO polymer sensors. Laser-to-sample-to-OSA are all connected by optical fibers (blue line). SG, signal generator; PC, polarization controller; OSA, optical spectrum analyzer.

To fabricate the antenna, the samples were evaporation coated with Ti/Au (20nm/100nm) as the seed layer for electroplating. The bowtie antenna was patterned using the MA6 and AZ P4620 photoresist. $2-2.5\mu$m of gold were electroplated onto the sample using a non-cyanide gold solution (Techni-Gold 25ES) at a temperature of $60°$C with a current density of 1 mA/cm for 20-30 minutes. The photoresist was removed using PG remover (Microchem) and the seed layers were wet-etched using commercially available etchants (Transene). Before spinning the top cladding layer, a second adhesion promoting layer is added. The top cladding is composed of an in-house sol-gel called 95/5 [11]; it is spun onto the sample and UV cured with a 10μm thickness. Sol-gel is used to prevent material breakdown during poling and also raises the optical mode closer to the electrodes to improve the antenna's field enhancement.

The sample was diced to a total length of about 1×1cm and insertion loss measurements were conducted before poling. A lensed fiber was used to couple into the waveguide and a microscope objective was used to couple out of the sample into a power meter or IR camera. The insertion loss of the device at 1550nm wavelength was measured to be 14dB for TE mode. During poling, the antennas were used as the contacts. Poling was performed under a nitrogen atmosphere with an applied voltage of 525V for 7μm electrode separation to a maximum temperature of $127°$C. The electrodes separation was narrower than designed due to over-exposure of the electroplating photoresist. The insertion loss after poling was 22dB for TE mode. We have previously observed an increase in insertion loss due to poling (5-10dB) [15] and a suggested cause is space-charge-induced inhomogeneous field distribution during poling [18]. The decreased electrode separation could also have led to increased loss from the electrodes. The sample was then pigtailed with the UHNA1-SM28 transition fiber for a total device insertion loss of $\sim$28dB.

B. Measurement and Result

The performance of the fabricated device was measured using the setup shown in Fig. 10. The device is connected to a 1550nm semiconductor laser and the output signal is connected to an optical spectrum analyzer (OSA). A MMW signal is created by a MMW signal generator which is then amplified and radiated with a horn antenna. The horn antenna (Mi-Wave) operates in the X-band at 10GHz and is positioned such that it radiates the MMW signal normal to the plane of the device. The distance between the horn and the device was 12 inches. The OSA (Yokogawa AQ6370C) has a 0.02nm resolution and a noise floor of -90dBm. A fiber polarization controller (PC) is used before the device to attain TE input for efficient MMW-optical signal conversion.

Typical spectra for the optical signal are shown in Fig. 11. The spectra are for the cases of no MMW signal irradiating the sample (blue dashed) and with a 11GHz MMW signal (red solid). The spectra are plotted over a shifted frequency defined as $\delta = f - f_0$, where f_0 is the optical frequency of 1550nm light. We found that MMW signals $<$ 10GHz would generates sidebands well within the laser bandwidth and were not visible by the OSA. This prevented us from seeing the sidebands at the simulated optimized signal of 5GHz. The device was able generate sidebands for MMW signals ranging from 10-14GHz. No sidebands were visible for frequencies $>$ 14GHz. Since the sidebands were within the bandwidth of the laser,

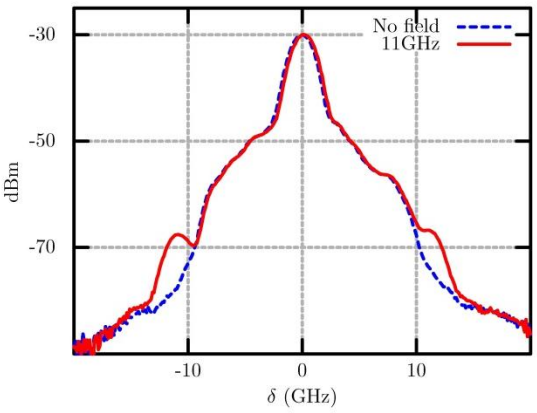

Fig. 11. OSA output for the fabricated device with no incident MMW radiation (blue dashed) and with 11GHz radiation (red solid).

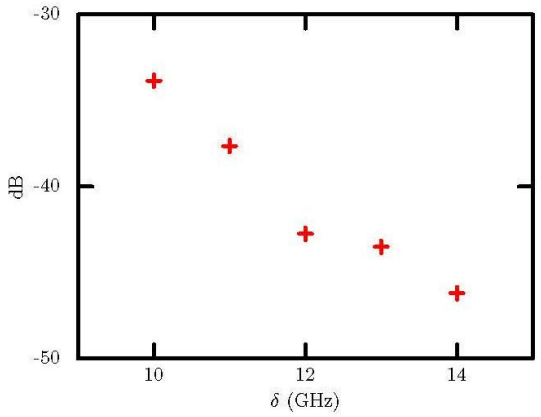

Fig. 12. Measured conversion efficiency (in dB) with respect to incident MMW signal.

the carrier spectrum was subtracted to the spectra collected at the different MMW signal to gather a corrected I_{FSB}. The peak difference between the carrier and the sidebands were calculated as a measure of the conversion efficiency of the device and is plotted in Fig. 12. The conversion efficiency reduces as the MMW frequency increases which correlates with the enhancement factor performance of the bowtie antenna as seen in Fig. 6. The conversion efficiency is between -33dB and -46dB for MMW signals in 10-14GHz range. To test the performance of the horn antenna at these frequencies, we replaced our device with a second horn antenna with the same specification and connected to a network analyzer. The signal was relatively uniform and clearly not a significant contributor to the observed frequency dependence.

VII. Conclusion

In this paper, we have presented the design, fabrication, and characterization of a silica/EO polymer phase modulator with an embedded bowtie antenna used for MMW receiving. The device is fabricated on silica for low RF reflection and high sensitivity. The bowtie antenna design simulations showed extremely broadband response and correlates well with measured data. This is the first MMW modulator receiver to incorporate EO polymer as the active material. The device is compact, pigtailed with SMF-28 fiber for ease of integration, and requires only straightforward fabrication techniques for both the waveguide and the electrodes. This device presents itself as an initial benchmark for future EO polymer-based MMW receivers and displays potential for a wide range of MMW detection due to its intrinsically fast electronic response. The device's applications can range from RF photonic links, electromagnetic field measurement, phased array radar, and radio-over-fiber technology. Future work will focus on reducing the insertion loss and further increasing the sensitivity.

VIII. Acknowledgment

This work was supported by the Air Force Office of Scientific Research through Phase I STTR contract FA8650-12-M-5132 and the NSF Center for Integrated Access Networks (CIAN) through grant #EEC-0812072.

References

[1] A. Yaghjian, "An overview of near-field antenna measurements," *Antennas and Propagation, IEEE Transactions on*, vol. 34, no. 1, pp. 30–45, 1986.

[2] V. B. Baglikov, R. Y. Dolinin, E. M. Zolotov, V. M. Pelekhatyĭ, and R. F. Tavlykaev, "Investigation of an electric field sensor based on an integrated optical mach-zehnder modulator," *Soviet Journal of Quantum Electronics*, vol. 18, no. 10, pp. 1353–1355, 1988.

[3] C. A. Schuetz and D. W. Prather, "Optical upconversion techniques for high-sensitivity millimetre-wave detection," pp. 166–174, 2004.

[4] C. J. Huang, C. Schuetz, R. Shireen, T. Hwang, S. Shi, and D. W. Prather, "Development of photonic devices for mmw sensing and imaging," 2006.

[5] C. J. Huang, C. A. Schuetz, R. Shireen, S. Shi, and D. W. Prather, "$LiNbO_3$ optical modulator for mmw sensing and imaging," p. 65480I, 2007.

[6] W. Bridges, F. Sheehy, and J. Schaffner, "Wave-coupled linbo3 electrooptic modulator for microwave and millimeter-wave modulation," *Photonics Technology Letters, IEEE*, vol. 3, no. 2, pp. 133–135, 1991.

[7] B. Sun, F. Chen, K. Chen, Z. Hu, and Y. Cao, "Integrated optical electric field sensor from 10 khz to 18 ghz," *Photonics Technology Letters, IEEE*, vol. 24, no. 13, pp. 1106–1108, 2012.

[8] N. Kohmu, H. Murata, and Y. Okamura, "Electro-optic modulators using double antenna-coupled electrodes for radio-over-fiber systems," *IEICE Trans. Electron*, vol. E96-C, no. 2, pp. 204 –211, 2013.

[9] Y. Wijayanto, H. Murata, and Y. Okamura, "Electrooptic millimeter-wave-lightwave signal converters suspended to gap-embedded patch antennas on low- k dielectric materials," *Selected Topics in Quantum Electronics, IEEE Journal of*, vol. 19, no. 6, pp. 33–41, 2013.

[10] M. Lee, H. E. Katz, C. Erben, D. M. Gill, P. Gopalan, J. D. Heber, and D. J. McGee, "Broadband modulation of light by using an electro-optic polymer," *Science*, vol. 298, no. 5597, pp. 1401–1403, 2002.

[11] Y. Enami, C. T. DeRose, D. Mathine, C. Loychik, C. Greenlee, R. A. Norwood, T. D. Kim, J. Luo, Y. Tian, A. K.-Y. Jen, and N. Peyghambarian, "Hybrid polymer/sol-gel waveguide modulators with exceptionally large electro-optic coefficients," *Nat Photon*, vol. 1, no. 13, pp. 180–185, 2007.

[12] Y. Enami, D. Mathine, C. DeRose, R. A. Norwood, J. Luo, A. K. Y. Jen, and N. Peyghambarian, "Hybrid cross-linkable polymer/sol-gel waveguide modulators with 0.65v half wave voltage at 1550nm," *Applied Physics Letters*, vol. 91, no. 9, pp. 093 505–093 505–3, 2007.

[13] W. H. Steier, A. Chen, S.-S. Lee, S. Garner, H. Zhang, V. Chuyanov, L. R. Dalton, F. Wang, A. S. Ren, C. Zhang, G. Todorova, A. Harper, H. R. Fetterman, D. Chen, A. Udupa, D. Bhattacharya, and B. Tsap, "Polymer electro-optic devices for integrated optics," *Chemical Physics*, vol. 245, no. 1–3, pp. 487 – 506, 1999.

[14] I. E. Araci, R. Himmelhuber, C. T. DeRose, J. D. Luo, A. K. Y. Jen, R. A. Norwood, and N. Peyghambarian, "Alignment-free fabrication of a hybrid electro-optic polymer/ion-exchange glass coplanar modulator," *Opt. Express*, vol. 18, no. 20, pp. 21 038–21 046, Sep 2010.

[15] R. Himmelhuber, O. D. Herrera, R. Voorakaranam, L. Li, A. Jones, R. A. Norwood, J. Luo, A. Jen, and N. Peyghambarian, "A silicon-polymer hybrid modulator - design, simulation and proof of principle," *Journal of Lightwave Technology*, vol. PP, no. 99, pp. 4067 – 4072, 2013.

[16] B. Saleh and M. Teich, *Fundamentals of Photonics*, 2nd ed. John Wiley, 2007.

[17] Y. Shi, L. Yan, and A. Willner, "High-speed electrooptic modulator characterization using optical spectrum analysis," *Lightwave Technology, Journal of*, vol. 21, no. 10, pp. 2358–2367, 2003.

[18] S. Huang, T.-D. Kim, J. Luo, S. K. Hau, Z. Shi, X.-H. Zhou, H.-L. Yip, and A. K. Y. Jen, "Highly efficient electro-optic polymers through improved poling using a thin TiO_2-modified transparent electrode," *Applied Physics Letters*, vol. 96, no. 24, pp. 243 311–243 311–3, 2010.

LIST OF ACRONYMS, ABBREVIATIONS, AND SYMBOLS

Acronym	Definition
EO	Electro-optic
MMW	Millimeter-wave
RF	Radio Frequency
FE	Field Enchancement
RIE	Reactive Ion
OSA	Optical Spectrum Analyzer
CIAN	Center for Integrated Access Networks